JOURNAL OF SPACECRAFT AND ROCKETS
Vol. 46, No. 6, November–December 2009

# Experiment on Drag Enhancement for a Blunt Body with Electrodynamic Heat Shield

Masaaki Kawamura*
*University of Tokyo, Tokyo 113, Japan*
Atsushi Matsuda† and Hiroshi Katsurayama‡
*Japan Aerospace Exploration Agency, Kanagawa 229, Japan*
Hirotaka Otsu§
*Shizuoka University, Shizuoka 432, Japan*
Detlev Konigorski¶
*EADS Space Transportation, GmbH, D-28199 Bremen, Germany*
and
Shunichi Sato** and Takashi Abe††
*Japan Aerospace Exploration Agency, Kanagawa 229, Japan*

DOI: 10.2514/1.44230

**The electrodynamic heat-shield technique, which is known as a potential alternative to the conventional thermal protection system in a reentry flight, enables us to control directly a partially ionized plasma flow in a shock layer as a result of the interaction between the flow and a magnetic field applied around a reentry vehicle. The origin of the interaction is the Lorentz force generated by the magnetic field. As a result of the control, we can expect not only a shock-layer enhancement, which causes heat flux mitigation, but also a reaction force to the vehicle in which the magnetic field generator is mounted. Such a reaction force causes a drag enhancement for the vehicle. In the present study, we experimentally verify not only the drag enhancement but also the integrated Lorentz force, which is the main cause for the drag enhancement. This experimental verification is a direct corroboration of the interaction that is a basis of the electrodynamic heat-shield technique.**

## I. Introduction

FOR a future space transportation system, a reusable system is desirable from the viewpoint of cost reduction and operational efficiency. A key issue for developing such a system is how to avoid or withstand a severe aerodynamic heating environment induced by a high-temperature gas flow around the vehicle during a reentry flight. Currently, to protect the vehicle from such high aerodynamic heating, only passive methods using an ablator, heat-resistant materials, adiabatic materials, and so on have been employed. Such a conventional thermal protection system (TPS), however, would need to be repaired and refurbished for the next flight. Hence, it is not suitable for a reusable space transportation system. Other than a conventional TPS, several active methods may be feasible to protect the vehicle. An electrodynamic heat-shield technique is among them. According to that technique, a high-temperature, and thus partially ionized, plasma flow around the vehicle can be controlled by applying a magnetic field around the vehicle [1]. As a result of such a flow control, a shock layer should be enhanced, and high convective heating may be reduced.

Phenomena associated with the electrodynamic heat-shield technique were actively investigated in the mid-1950s and 1970s [2–5], both theoretically and experimentally. Kranc et al. [2] measured a drag force for the magnetized blunt body in the argon plasma flow and found an enhancement of drag force caused by the magnetic interaction with the ionized flow. Nowak and Yuen [5] investigated the heat flux to a body located in the argon plasma flow and the effect of the applied magnetic field on the plasma flow, and they reported the heat flux reduction caused by the electromagnetic effect. In their experiment, however, the heat measurement sensor might have been affected by the strong magnetic field. Ziemer [3], Ziemer and Bush [4], Nowak and Yuen [5], and Nowak et al. [6] investigated shock front modification through the application of a magnetic field by visualizing the self-radiating flow around a body. Concomitantly, Nowak and Yuen [5] and Nowak et al. [6] reported a significant effect on the luminosity of the region even in front of the shock wave, that is, because of the magnetic field application in front of the model, the luminous region is enhanced even in the region ahead of the shock wave. In spite of their effort to understand the electrohydrodynamic phenomenon, ambiguities have remained. In addition, the electrodynamic heat-shield technique was not considered practical in those days, because a strong magnetic field generator mountable on a spacecraft was not available. Nevertheless, recent advancements of new technology for superconducting materials may enable us to produce a strong magnetic field generator for space application. Because of this technology advancement, this electrodynamic heat-shield technique has been revisited recently, and new theoretical (numerical) and experimental investigations have begun [7–9].

By using the numerical simulation technique, Poggie and Gaitonde demonstrated the shock-layer enhancement phenomenon caused by the applied magnetic field [10]. After that, numerous numerical

Presented as Paper 3889 at the 38th AIAA Plasmadynamics and Lasers Conference, Miami, FL, 25–28 June 2007; received 9 March 2009; revision received 28 July 2009; accepted for publication 9 September 2009. 

*Graduate Student, Department of Aeronautics and Astronautics, 7-3-1 Hongo Bunkyouku. Member AIAA.
†Postdoctoral Researcher, Space Transportation Engineering Division, Institute of Space Astronautical Science, 3-1-1 Yoshinodai, Sagamihara. Member AIAA.
‡Postdoctoral Researcher, Space Transportation Engineering Division, Institute of Space Astronautical Science, 3-1-1 Yoshinodai, Sagamihara. Member AIAA.
§Research Associate, Department of Mechanical Engineering, 3-5-1 Johoku, Hamamatsu. Member AIAA.
¶Technical Engineer. Member AIAA.
**Technical Staff, Space Transportation Engineering Division, Institute of Space Astronautical Science, 3-1-1 Yoshinodai, Sagamihara.
††Professor, Space Transportation Engineering Division, Institute of Space and Astronautical Science, 3-1-1 Yoshinodai, Sagamihara. Associate Fellow AIAA.

studies were carried out based on a similar magnetohydrodynamic (MHD) equation. Matsushita et al. [11,12] pointed out that the magnetic interaction effect is effective in the real reentry flight condition and, in addition, that the Hall effect may not be negligible during the flight. Otsu et al. [13,14] and Fujino [15] investigated the Hall effect critically and concluded that, for the insulated model, the shock layer can be enhanced because of the applied magnetic field and the heat reduction effect can be expected. On the other hand, for the conductive surface, the interaction effect between the magnetic field and the plasma is almost entirely canceled out, and the effect of enhancing the shock-layer width cannot be expected. In addition to studying the Hall effect, Otsu et al. [13,14] investigated the magnetic field configuration effect on the phenomenon. They pointed out that the shock-layer enhancement effect is more enhanced in the blunt-nose configuration than in the flat-nose configuration [16,17]. Takizawa et al. [18–21] and Matsuda et al. [22–24] investigated the interaction between applied magnetic fields and weakly ionized plasmas by means of an arcjet wind tunnel. They measured translational temperature ahead of a flat-faced model by means of laser absorption spectroscopy [21]. Measured translational temperature distribution along the stagnation line clearly showed shock-layer enhancement caused by the applied magnetic field. Based on a similar technique, they successfully verified not only the Hall effect but also the magnetic field configuration effect, both of which were previously suggested theoretically [22–24].

Besides shock-layer enhancement, the interaction is expected to cause drag enhancement of the model. As an interaction of the applied magnetic field generated around the model with weakly ionized flow ahead of the model, the Lorentz force appears and pushes weakly ionized flow away from the model. As a reaction to the Lorentz force, the source of the magnetic field generation mounted inside the model should be pushed back. Because the Lorentz force is distributed in the flow, the source of the magnetic field experiences an integration of the Lorentz force. This integration may cause enhancement of the total drag for the model. Numerically, this enhancement of the total drag has been predicted successfully [17,25]. Hence, experimental validation of total drag enhancement is necessary. Such experimental validation is critical because it gives us further justification for the electrodynamic heat-shield technique in addition to validation of the shock-layer enhancement phenomenon that has been carried out successfully [21]. Experimental validation of the Lorentz force itself is especially important because the Lorentz force is the main cause of total drag enhancement, as well as the main cause of shock-layer enhancement.

In the present study, we measure the drag force acting on the spherically blunted body model. Besides drag force, we measure the integrated Lorentz force. Using those measurements, we clarify direct evidence of the electrohydrodynamic interaction on which the electrodynamic heat-shield technique is based.

## II. Experimental Setup

### A. Arcjet Wind Tunnel

To produce a weakly ionized supersonic flow, an arcjet wind tunnel is employed. For the wind tunnel, an arc heater with a nozzle is installed in an evacuated chamber. We use a normal-type arc heater with an input power of 1.5 kW. Argon gas was employed as a test gas because of the simplicity of its application. Argon gas that is arc heated at a plenum is expanded through a conical nozzle with a throat diameter, half-angle, and exit diameter of 3 mm, 25 deg, and 30 mm, respectively. The evacuation chamber has a cylindrical configuration with dimensions of 0.5 m in diameter and 1.6 m in length, and it maintains its pressure at less than 13 Pa during testing. The specifications for typical flow conditions at the location where the model is inserted (110 mm downstream from the nozzle exit) are summarized in Table 1. To determine these characteristics of the flow, several measurements were carried out [26,27]. To determine the Mach number, the pressure ratio between the total and the static pressures was measured by a pitot tube, and the electron temperature and density were determined by means of a single probe method [27].

**Table 1 Test flow conditions**

| Test gas | Argon |
|---|---|
| Mach number | ∼1.7 |
| Max total enthalpy, MJ/kg | 1.1 |
| Total pressure, Pa | 160 |
| Static pressure, Pa | 34 |
| Electron temperature, K | 10000 |
| Electron density, $m^{-3}$ | $1.0 \times 10^{19}$ |
| Mean freepath, mm | ∼2.0 |

### B. Test Models

In this experiment, we used a spherically blunted body model, as shown in Fig. 1. The head (painted in gray) of the model is made of a ceramic material (Marcor) to resist high-temperature plasma flow and to prevent heating up of the inner part of the model. The remainder of the model (i.e., other than the head) is made of Bakelite. The model was located 110 mm downstream from the nozzle exit.

Permanent magnets composed of three pieces are installed inside the model to generate a strong magnetic field at the head of the model. One piece has a spherical configuration with a diameter of 15 mm $\phi$, while the other two pieces are a cylindrical configuration with dimensions of 15 mm $\phi$ in diameter and 10 mm in height. The three magnetic pieces are connected in tandem to generate a strong magnetic field at the head of the model, as shown in Fig. 1. The permanent magnet is composed of neodymium, and it is magnetized in an axial direction of the model. Distribution of the magnetic field around the model is depicted in Fig. 1 and is described in detail in [23]. Table 2 summarizes the specifications of the models used in this experiment. We employed three types of models that differ in their magnetic field strength at the model head. The magnetic field strength $B_s$ at the head of the models or at its stagnation point is 0 T for the S22-CER model, 0.1 T for the S22-CER-M01 model, and 0.4 T for the S22-CER-M04 model. For models S22-CER and S22-CERM01, the permanent magnets are intentionally demagnetized; therefore, the permanent magnets in the models have identical physical properties except for the magnetic field strength. Comparing the results among models S22-CER-M04, S22-CER-M01, and S22-CER, we can distinguish the pure magnetic field effect, because their physical properties are the same except for the magnetic field strength. Between the back surface of the ceramics at the head of the model and the surface of the magnet, a slight empty space is left to prevent demagnetization of the magnet that can result from temperature elevation during testing.

To evaluate the magnetic field effect for the electrodynamic heat-shield effect, it is useful to evaluate the interaction parameter $Q$ [19]:

$$Q = \frac{\sigma B^2 L_B}{\rho V} \tag{1}$$

which is a ratio of the Lorentz force to the flow inertial force. Here, $B$, $L_B$, $\rho$, and $V$ are the magnetic field strength, the body size, the density of the flow, and the flow velocity, respectively. Assuming typical flow conditions ($T_t \sim 2000$ K, a static pressure of 34 Pa, and a flow

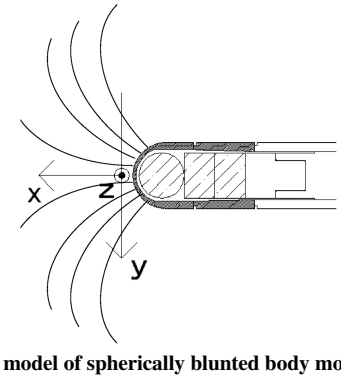


**Fig. 1 Test model of spherically blunted body model (top view).**

**Table 2 Specifications of spherically blunted body models**

| Model | Diameter | $B_s$ |
|---|---|---|
| S22-CER-M04 | 22 mm | 0.4 T |
| S22-CER-M01 | 22 mm | 0.1 T |
| S22-CER | 22 mm | 0 |

velocity of 1400 m/s), we can evaluate the interaction parameter $Q$ as 43 under these test conditions for model S22-CER-M40, based on typical electrical conductivity $\sigma$ of 1400 $[\Omega m]^{-1}$. Theoretically speaking, this value is adequate to observe the drag increase effect.

### C. Measurement System

*1. Total Drag*

An experimental setup for drag force measurement is shown schematically in Fig. 2. A pendulum system was adopted to hold the model vertically and to enable us to measure the force in the horizontal direction, that is, we can measure the force acting on the model along the drag force direction. The test model was held by a 5-mm-diam stainless steel rod *A* that was attached to the support structure using a pivot. To minimize friction at the pivot of the pendulum, a mechanical joint with ball bearings was used. As a sensor for the force measurement, we used a load cell mounted at a location where the sensor was not influenced by partially ionized plasma flow. We chose load cell LVS-50GA (Kyowa Electronic Instruments Company, Ltd., Japan); the specifications are summarized in Fig. 2. The maximum range of this load cell is 500 mN. An infinitesimal displacement of rod A caused by the force acting on the model is transferred to the load cell through rod B, which is attached to rod A. The total pendulum system was mounted inside the vacuum chamber, along with the model.

*2. Integrated Lorentz Force*

As an interaction of the applied magnetic field with the weakly ionized flow ahead of the model, the Lorentz force appears and pushes the weakly ionized flow away from the model. As a reaction to the Lorentz force, the permanent magnet receives a force in a reversed direction. Because the Lorentz force is a body force distributed in the flow, the magnet inside the model feels the integrated Lorentz force as a reaction and is pushed back. This reaction causes enhancement of the total drag of the model.

In the present experimental setup, measurement of the integrated Lorentz force can be conducted by directly measuring the force acting on the permanent magnet mounted inside the model. To measure the force acting on the permanent magnet, the permanent magnet inside the model is mechanically separated from the outer shell of the model, and only the permanent magnet is mounted on the pendulum system while the outer part of the model is supported separately, as shown in Fig. 3. Otherwise, the measurement setup is similar to that for total drag. In this configuration, the value measured by the pendulum system should be only for the force acting on the permanent magnet because there is no mechanical contact between the permanent magnet and the outer part of the model. Nevertheless it should be noted that this force can be influenced by the aerodynamic force acting on a part of rod A and the extended part of rod A (or the base part of the model). Therefore, those components of the aerodynamic force must be subtracted from the measured value if they are not small enough.

*3. Calibration*

To correlate the voltage output of the load cell with the drag force acting on the model, a calibration is necessary. Calibration of the pendulum measurement system is conducted by applying a specified force to the model horizontally, or parallel, to the flow direction. A specific force is generated by a specified weight using a fixed pulley, as shown in Fig. 2. The calibration curve for the output voltage of the load cell is linear with reasonable applied force, as shown in Fig. 4. From this calibration curve, we can determine the force acting on the model.

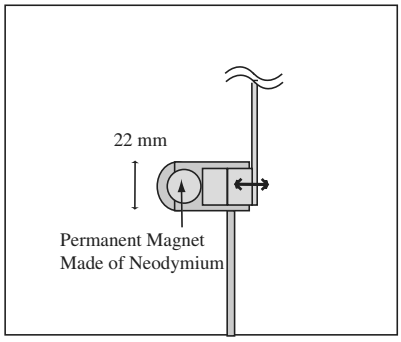


**Fig. 3 Schematic of integrated Lorentz force measurement setup.**

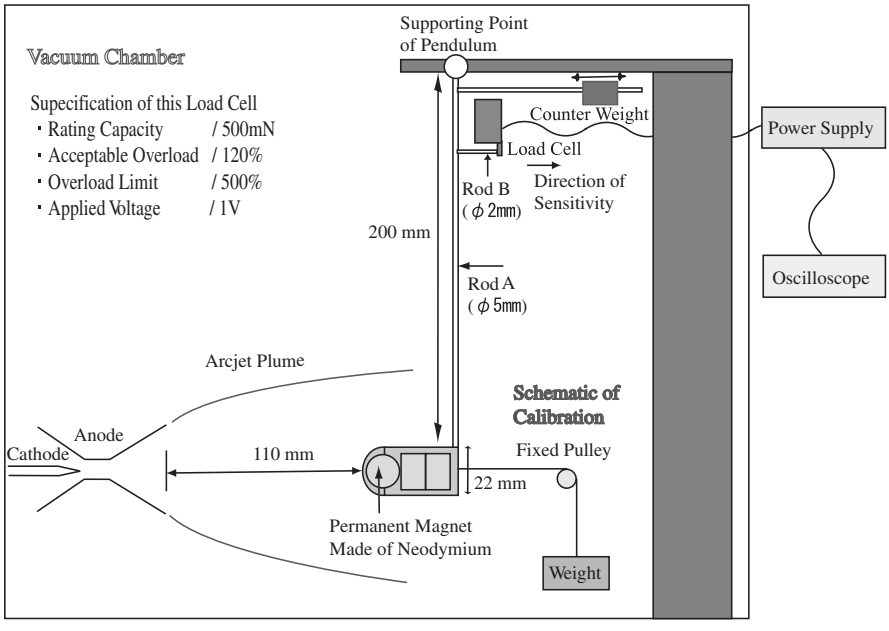


**Fig. 2 Schematic of drag force measurement setup.**

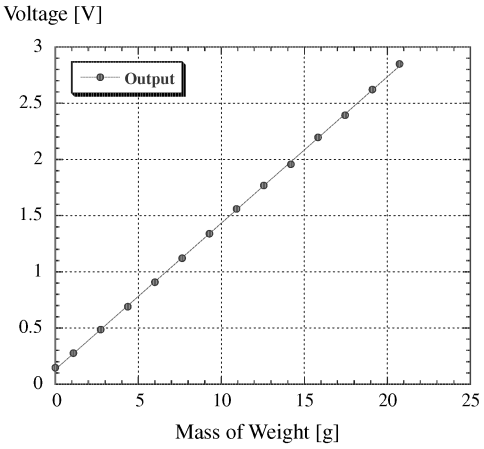


**Fig. 4 Calibration curve.**

## III. Numerical Predictions

Under the test flow conditions specified in Table 1, the total drag as well as the integrated Lorentz force were predicted numerically for the magnetized model specified in Table 2 [25]. For the numerical simulation, the magnetohydrodynamic equation was solved by assuming a low magnetic Reynolds number and neglecting a magnetic field modification by the plasma flow. For the electric current, the generalized Ohm's law was assumed. For the hydrodynamic part of the equation, the direct simulation Monte Carlo (DSMC) method was applied because the flow is in a slightly rarefied regime, as shown in Table 2. Note that even the standard MHD analysis gives a result similar to that obtained by the DSMC simulation because the rarefied effect is relatively weak. The axial force exerted on the model is composed of the aerodynamic and integrated Lorentz force portions. Furthermore, the aerodynamic portion can be classified as the force exerted on the spherical, cylindrical, and base part of the model. In Fig. 5, each component of the axial force is identified with its raw value. Because the flow is in a weakly rarefied regime, the axial force exerted on the cylindrical part is comparable to the force exerted on the spherical part. To visualize clearly the contribution of the integrated Lorentz force and the aerodynamic force, only the integrated Lorentz force portion and the aerodynamic force portion are presented in Fig. 6, in which each axial force, $F$, is converted to nondimensional form (the so-called the drag coefficient), $C_D$:

$$C_D = \frac{F}{(1/2)\rho V^2 S} \tag{2}$$

where $\rho$ and $V$ are the flow density and speed, respectively, and $S$ is a representative area defined as a cross area of the cylindrical part of the model. As the magnetic field strength increases, the total drag coefficient increases. This relationship is caused mainly by the increase in the integrated Lorenz force portion, whereas the aerodynamic force portion decreases slightly.

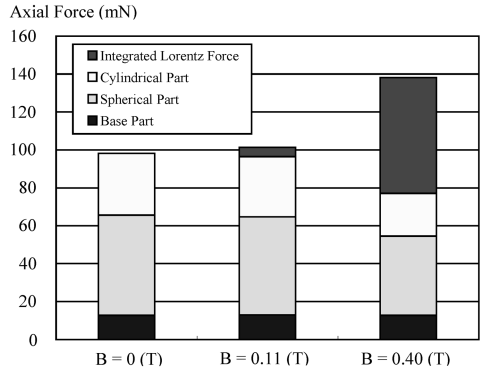


**Fig. 5 Numerical prediction of components of axial force under experimental conditions of this study.**

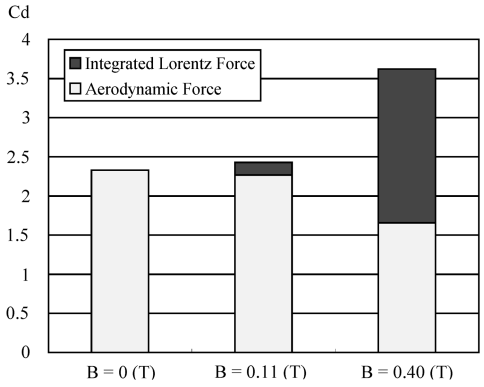


**Fig. 6 Numerical prediction of total drag coefficient and its aerodynamic and Lorentz force components under experimental conditions of this study.**

## IV. Experimental Results and Discussion

### A. Total Drag

In our experiment, the arcjet flow is, at the beginning, prevented from hitting the model by means of a shutter placed in front of the model. Then the shutter is promptly activated to open, and the arcjet flow hits the model instantly; therefore, the drag force will appear instantaneously. A few seconds later, the arcjet flow is switched off. For this short exposure time, the surface of the model is inevitably heated up. But the heating of the permanent magnet mounted inside the model is not significant enough to deteriorate the magnetic performance of the permanent magnet. Furthermore, we should note that, during testing, the model may be affected by vibration of the chamber itself because the vacuum pump located near the chamber is continuously running during the experiment, which may cause undesirable vibration of the test chamber. In fact, measurement results show that this is the case, that is, even before the flow hits the model, a large fluctuation can be observed everywhere in the signal of the load cell, as shown in Fig. 7. Nevertheless, a clear jump can be observed in the signal once the flow hits the model. To minimize such a fluctuation effect on the signal, we designed a proper numerical filter. For this purpose, a fast Fourier transform (FFT) analysis was applied to the original signal, as shown in Fig. 8. According to the FFT analysis, the main component of the noise is around 8 Hz. Therefore, we applied a numerical filter that deletes all frequency components greater than 5 Hz, from the original signal, as depicted in Fig. 7. This signal clearly shows a jump caused by the application of the flow to the model. The difference of the output voltage at the jump can be converted to the force acting on the model, based on the

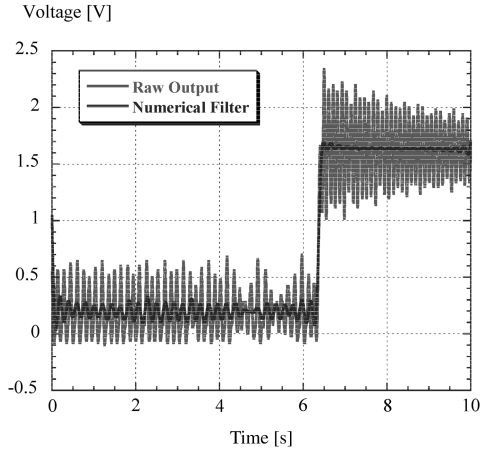


**Fig. 7 Typical raw output signal for total drag measurement.**

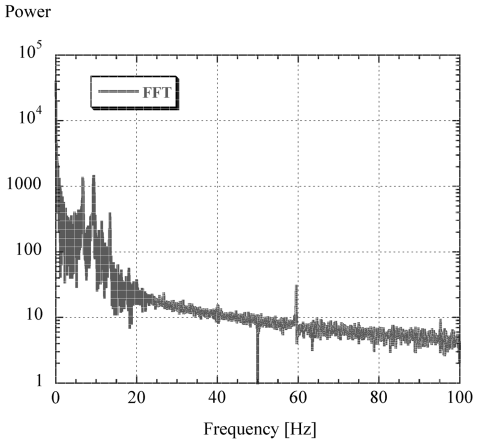


**Fig. 8 Spectrum of typical output signal of load cell.**

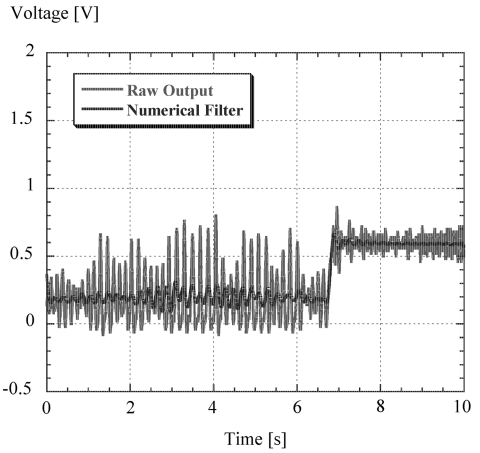


**Fig. 10 Typical raw output signal for integrated Lorentz force measurement.**

calibration curve described earlier. In the present setup of the model, the force thus measured may be influenced by the aerodynamic force acting on the part of rod A supporting the model because it is exposed to the flow. Nevertheless this influence can be expected to be negligible, as we will discuss in the next subsection. The force acting on the model, $F$, is converted to the drag coefficient, $C_D$.

The drag coefficients thus determined for the models with various magnetic field strengths are depicted in Fig. 9, in which the value averaged over four measurements is depicted and the error bar is determined as a scatter among the four measurements. As expected, the drag for the model with magnetic field increases with increasing magnetic field strength. In the past, Kranc et al. [2] measured a drag force for the magnetized blunt body in the arcjet wind tunnel and found an enhancement of drag force caused by the magnetic interaction with the ionized flow. Nevertheless, their experimental setup was far more complex than our system. In fact, their model was magnetized by an electromagnetic coil with a large electric current. Because of this, the liquid coolant had to be circulated inside the model. The complexity of their setup may have had an adverse effect on their measurements. In spite of this difficulty, their results show a the drag enhancement of 27% at the interaction parameter of 43, which is comparable to our result of 26% at the same interaction parameter.

### B. Integrated Lorentz Force

The measurement for the integrated Lorentz force was carried out in a manner similar to that for total drag measurement. The typical output signal of the load cell and the numerically filtered signal are depicted in Fig. 10. We can observe a similar jump in the signal, which is caused by onset of the flow. Similarly, the height of the jump can be converted to the force. The converted force for each model is shown in Fig. 11. As mentioned earlier, this force is composed of the force acting not only on the permanent magnet but also on the part of rod A exposed to the flow and the extended part of the model connected to rod A. For this reason, a certain drag force appears even for the model without the magnetic field. Therefore, the integrated Lorentz force acting on the permanent magnet can be evaluated by subtracting the force that appears for the model without the magnetic field. The integrated Lorentz force thus determined for each case is shown in Fig. 12, in which the value averaged over four measurements is depicted and the error bar is determined as a scatter among the four measurements. As we expected, the integrated Lorentz force increases with increasing magnetic field strength.

The certain drag force appearing for the model without the magnetic field, which amounts to $\sim$13.5 mg as indicated in Fig. 11, is almost equivalent to an amount of the base part ($\sim$14 mg) that is predicted numerically as indicated in Fig. 5. Thus, we can expect that the influence of the part of rod A exposed to the flow is small enough.

By subtracting the integrated Lorentz force from the total drag, we can evaluate the aerodynamic portion of the total drag. The aerodynamic portion thus determined and the integrated Lorentz force for each case are depicted in Fig. 13.

### C. Comparison with Numerical Prediction

To discuss our experimental results, the numerical simulation results obtained previously [25] are useful. In the simulation, the rarefied effect was taken into account by using the DSMC method. In return, only a simple model for the MHD effect is incorporated. In the numerical simulation, it is assumed that the magnetic field is generated by a dipole magnet inside the model. Concerning the

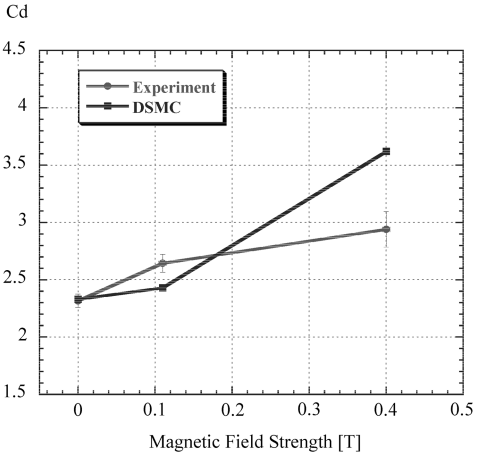


**Fig. 9 Total drag coefficient.**

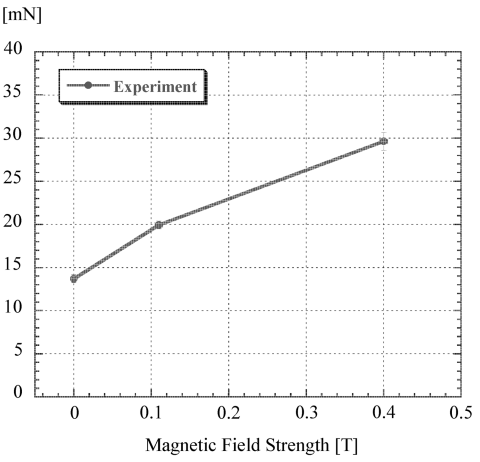


**Fig. 11 Value before correction for integrated Lorentz force measurement.**

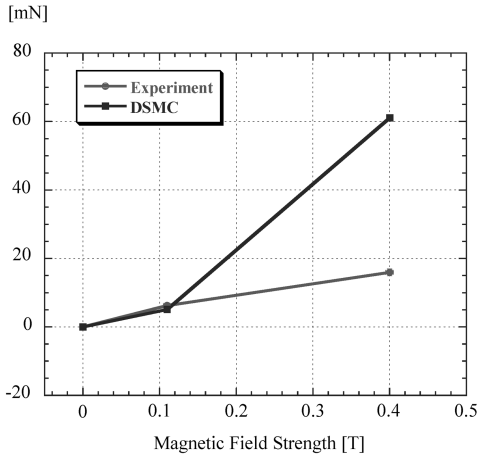


**Fig. 12 Integrated Lorentz force.**

magnetic field distribution around the model, however, this assumption is acceptable as discussed previously [23].

The prediction by the DSMC simulation [25] is shown in Fig. 9; the DSMC and numerical predictions show good agreement, especially in qualitative terms. The prediction based on the DSMC method [25] is depicted in Fig. 12; in this case too, the methods show good agreement in qualitative terms, that is, with increasing magnetic field strength, not only the drag force but also the integrated Lorentz force increases. Quantitatively, however, they show discrepancy, that is, the numerical prediction slightly overestimates both forces with increasing magnetic field strength. In contrast, the aerodynamic portion shows, even in a quantitative terms, good agreement with the numerical prediction shown in Fig. 6. Therefore, the quantitative discrepancy observed in the drag force is attributable to the discrepancy observed in the integrated Lorentz force portion; in other words, the integrated Lorenz force is overestimated in the numerical prediction. Apart from the measurement error, the reason for this discrepancy can be explained as follows.

In the numerical prediction, it is assumed that the Hall effect can be neglected and that uniform flow comes across the model. Under present experimental conditions, however, the Hall parameter with typical flow conditions ($T_t = 2000$ K, a static pressure of 34 Pa, a flow velocity of 1400 m/s, and a $B$ of 0.40 T) amounts to around 350, which is much larger than unity. Moreover, the flowfield coming across the model departs from uniform flow. Furthermore, flow generated in the arcjet wind tunnel is preionized even before the shock wave generated in front of the model. Recent intensive studies [28–30] have clarified somewhat the influence of the Hall effect and the influence of the nonuniform and weakly preionized flow generated in the arcjet wind tunnel. As Otsu et al. [14] and Fujino et al. [15] pointed out, the Hall effect has a significant effect on the shock standoff distance enhancement caused by the magnetic force, and it deteriorates the shock standoff distance enhancement. Moreover, Katsurayama et al. [28] pointed out that, in preionized

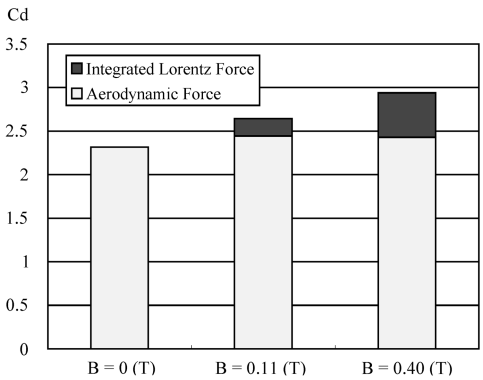


**Fig. 13 Measured values for total drag coefficient and its aerodynamic and Lorentz force components.**

flow, this degradation of the magnetic force effect can not be avoided even in the case in which the model surface is insulative, unlike the nonpreionized flow that was assumed by Otsu et al. and Fujino et al. In other words, the preionized flow effect somehow enhances the degradation of the shock standoff distance enhancement [28–30], which is clearly observed in nonpreionized flow if the flow is characterized by a large value of the Hall parameter. These results suggest that the integrated Lorentz force and, thus, a total drag enhancement may be affected in a similar manner and may be reduced to a smaller value. Beside the aforementioned phenomena, an enhancement of the luminous region even ahead of the shock wave, which was suggested previously [5,6], was observed. Our previous experimental results show that the electron excitation temperature at the region is reduced compared with the values without the magnetic effect [18]. Nevertheless, this phenomenon remains to be investigated and its effect on the present result must be investigated. In summary, to predict and evaluate the experimental results more precisely, further investigation is necessary.

## V. Conclusions

To validate drag enhancement in a weakly ionized flow with the application of a magnetic field, we measured the drag force acting on the spherically blunted body model in cases with and without the magnetic field. Compared with the case without the magnetic field, the drag force acting on the model increases in the case with the magnetic field, that is, the larger the magnetic field is, the larger the drag force is. Furthermore, we measured the integrated Lorentz force, which is the main cause for total drag force enhancement. The integrated Lorentz force increases with increasing magnetic field strength. The experimental total drag and integrated Lorentz force agree with the numerical predictions based on the DSMC simulation, at least qualitatively. An aerodynamic portion of the total drag, which is defined as the total drag minus the integrated Lorentz force portion, shows reasonable agreement with the prediction. On the contrary, the experimentally measured integrated Lorentz force portion does not increase as much as it should according to numerical predictions. Therefore, more detailed analysis must be carried out in the future.

## Acknowledgment

This research was partially supported by the Ministry of Education, Science, Sports, and Culture Grant-in-Aid for Scientific Research (A), 1820687, 2006.

## References

[1] Kantrowitz, R., "A Survey of Physical Phenomena Occurring in Flight at Extreme Speeds," in *Proceedings of the Conference on High-Speed Aeronautics*, edited by A. Ferri, N. J. Ho., and P. A. Libby, Polytechnic Inst. of Brooklyn, New York, 1955, pp. 335–339.

[2] Kranc, S., Yuen, M. C., and Cambel, A. B., "Experimental Investigation of Magnetoaerodynamic Flow Around Blunt Bodies," NASA CR-1393, 1969.

[3] Ziemer, R. W., "Experimental Investigation in Magneto-Aerodynamics," *ARS Journal*, Vol. 19, Sept. 1959, pp. 642–647.

[4] Ziemer, R. W., and Bush, W. B., "Magnetic Field Effects on Bow Shock Standoff Distance," *Physical Review Letters*, Vol. 1, 1958, pp. 58–59. doi:10.1103/PhysRevLett.1.58

[5] Nowak, R. J., and Yuen, M. C., "Heat Transfer to a Hemispherical Body in a Supersonic Argon Plasma," *AIAA Journal*, Vol. 11, No. 11, 1973, pp. 1463–1464. doi:10.2514/3.50611

[6] Nowak, R., Kranc, J. S., Porter, R. W., Yuen, M. C., and Cambel, A. B., "Magnetoaerodynamic Re-entry," AIAA Paper 1966-161, 1996.

[7] Shang, S., Hayes, J., Harris, S., Umstattd, R., and Ganguly, B., "Experimental Simulation of Magneto-Aerodynamic Hypersonics," AIAA Paper 2000-2258, 2000.

[8] Hoffmann, K. A., Damevin, H. M., and Dietiker, J. F. "Numerical Simulation of Hypersonic Magnetohydrodynamic Flows," AIAA Paper 2000-2259, 2000.

[9] Bityurin, V., and Bocharov, A., "MHD Flow Control in Hypersonic Flight," AIAA Paper 2005-3225, 2005.

[10] Poggie, J., and Gaitonde, D. V., "Magnetic Control of Flow Past a Blunt

Body: Numerical Validation and Exploration," *Physics of Fluids*, Vol. 14, 2002, pp. 1720–1731.
doi:10.1063/1.1465424

[11] Matsushita, K., Takizawa, Y., and Abe, T., "Control of Aerodynamic Heating in Hypersonic Plasma Flow by Magnetic Field," ISTS Paper 2002-s-22, May 2002.

[12] Matsushita, K., "Reentry Hypersonic Flow Control by Means of Electro Magnetic Force," Doctoral Dissertation, Univ. of Tokyo, Tokyo, Dec. 2003.

[13] Otsu, H., Matsushita, K., Konigorski, D., Funaki, I., and Abe, T., "Reentry Heating Mitigation by Utilizing the Hall Effect," AIAA Paper 2004-2167, June 2004.

[14] Otsu, H., Abe, T., and Konigorski, D., "Influence of the Hall Effect on the Electrodynamic Heat Shield System for Reentry Vehicles," AIAA Paper 2005-5049, June 2005.

[15] Fujino, T., Funaki, I., Mizuno, M., Sugita, H., and Ishikawa, M., "Numerical Studies of Influences of Hall Effect on MHD Flow Control Around Blunt Body," AIAA Paper 2004-2561, June 2004.

[16] Otsu, H., and Abe, T., "Hall Effect for Aerodynamic Heating Reduction by Electrodynamic Heatshield Technique," (in translation) *37th Fluid Dynamics Conference*, Japan Society for Aeronautical and Space Science, Tokyo, Sept. 2005, pp. 61–64.

[17] Taniguchi, R., Otsu, H., Yoshiki, Y., Kawamura, M., Takizawa, Y., Matsuda, A., and Abe, T., "Numerical Investigation for Aerodynamic Drag Enhancement of Blunted Body by Applying Magnetic Field," (in translation) *38th Fluid Dynamics Conference*, Japan Society for Aeronautical and Space Science, Tokyo, Sept. 2006, pp. 153–156.

[18] Takizawa, Y., Matsushita, K., Sato, S., Fujita, K., Abe, T., and Konigorski, D., "Electromagnetic Effect on Reentry-Related High-Enthalpy Flow," AIAA Paper 2003-4168, 2003.

[19] Takizawa, Y., Sato, S., Abe, T., and Konigorski, D., "Electromagnetic Effect on Shock Layer Structure in Reentry-Related High-Enthalpy Flow," AIAA Paper 2004-2162, 2004.

[20] Takizawa, Y., Matsuda, A., Sato, S., Abe, T., and Konigorski, D., "Experiment on Shock Layer Enhancement by Electromagnetic Effect in Reentry-Related High-Enthalpy Flow," AIAA Paper 2005-4786, 2005.

[21] Takizawa, Y., Matsuda, A., Sato, S., Abe, T., and Konigorski, D., "Experimental Investigation of the Electromagnetic Effect on a Shock Layer Around a Blunt Body in a Weakly Ionized Flow," *Physics of Fluids*, Vol. 18, 2006, pp. 117105–117110.
doi:10.1063/1.2375076

[22] Matsuda, A., Wakatsuki, K., Takizawa, Y., Kawamura, M., Otsu, H., Sato, S., Abe, T., and Konigorski, D., "Shock Layer Enhancement by Electromagnetic Effect for Spherically Blunt Body," AIAA Paper 2006-3573, 2006.

[23] Matsuda, A., Otsu, H., Kawamura, M., Konigorski, D., Takizawa, Y., Sato, S., and Abe, T., "Model and Magnetic Configuration Effect on Shock Layer Enhancement by an Applied Magnetic Field," *Physics of Fluids*, Vol. 20, 2008, p. 027102.
doi:10.1063/1.2832782

[24] Matsuda, A., Otsu, H., Kawamura, M., Konigorski, D., Takizawa, Y., and Abe, T., "Model Surface Conductivity Effect for the Electromagnetic Heat Shield in Re-Entry Flight," *Physics of Fluids*, Vol. 20, 2008, p. 127103.
doi:10.1063/1.3054149

[25] Katsurayama, H., Kawamura, M., Matsuda, A., and Abe, T., "Kinetic and Continuum Simulations of Electromagnetic Control of a Simulated Reentry Flow," *Journal of Spacecraft and Rockets*, Vol. 45, No. 2, 2008, pp. 248–254.
doi:10.2514/1.31702

[26] Schönemann, A., Auweter-Kurtz, M., Dabalà, P., Fasoulas, S., Früholz, H., Habiger, H., Kurtz, H., Laure, S., Loesener, O., and Röck, W., "Plasma Wind Tunnels PWK1 and PWK2," Univ. of Stuttgart, IRS92-P6, 1992.

[27] Takizawa, Y., "Trial Production and Performance Testing for Reentry Environment Facility," (in translation) Master's Thesis, Univ. of Tokyo, Tokyo, 2000.

[28] Katsurayama, H., Abe, T., Otsu, H., and Konigorski, D., "Numerical Study of the Electromagnetic Control of a Weakly Ionized Flow around a Blunt Body: Role of an Insulative Boundary in the Flow," AIAA Paper 2007-4529, 2007.

[29] Katsurayama, H., Konigorski, D., and Abe, T., "Numerical Simulation of Electromagnetic Flow Control in an Arcjet Plume," AIAA Paper 2008-1392, 2008.

[30] Katsurayama, H., Konigorski, D., and Abe, T., "Numerical Simulation of Electromagnetic Flow Control in a One-Kilowatt Class Argon Arcjet Wind Tunnel," AIAA Paper 2008-4016, 2008.

I. Boyd
*Associate Editor*